ScientificScholar®
Knowledge is power
Publisher of Scientific Journals

https://arabjchem.org

Arabian Journal of Chemistry

2025 18 (12) 1582025

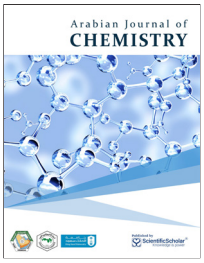

Original Article

# Metallochromic electrospun nanofibrous membrane of a biopolymer hybrid for chromogenic identification of ferric

Salhah D. Al-Qahtani[a,*], Arwa S. Alqahtani[b], Ghadah M. Al-Senani[a]

[a]Department of Chemistry, College of Science, Princess Nourah bint Abdulrahman University, P.O. Box 84428, Riyadh 11671, Saudi Arabia
[b]Department of Chemistry, College of Science, Imam Mohammad Ibn Saud Islamic University (IMSIU), P.O. Box 90950, Riyadh 11623, Saudi Arabia

ARTICLE INFO

*Keywords*:
Colorimetric determination of iron(III)
Electrospun nanofibrous membrane of polycaprolactone and polylactic acid
Tannic acid

ABSTRACT

Metallochromic nanofibrous membranes for the detection of iron(III) in aqueous solutions were developed from a composite of polycaprolactone and polylactic acid (PCL/PLA) as the hosting material and tannin as an active detection probe. The reported sensor is simple, easy to use, quick, portable, and accurate. The coloration parameters showed that binding the ferric ions to the phenol hydroxyl groups of the tannin probe resulted in an obvious change in colorimetry from 409 nm (colorless) to 580 nm (purple), demonstrating a bathochromic shift. A direct correlation was monitored between the ferric concentration and the visible color change. A coordination complex formed between $Fe^{3+}$ and phenolic tannin provided the rationale for the detection of ferric ions. Transmission electron microscopic (TEM) analysis of Tannin/$Fe^{3+}$ complex nanoparticles indicated diameters in the range of 6-23 nm. An average diameter of 100-420 nm was revealed for the electrospun nanofibrous film. The detection range was determined as 0.5-125 ppm, with a detection limit of 0.5 ppm. The tannin-encapsulated PCL/PLA has shown high selectivity as compared to other metallic salts. The optimum conditions for identification of $Fe^{3+}$ were monitored in the pH range of 4.0-6.5. In comparison to other detection techniques, the present assay is advantageous in terms of environmental safety, simplicity, rapidity, low cost, and ease of operation.

## 1. Introduction

Iron has been a major contaminant in water sources. It is the most prevalent heavy metal in the human body, as it has vital functions in biological organs [1,2]. Various proteins use iron as a catalytic agent in the oxidoreductase reaction and as an electron and oxygen-transporting agent. Owing to great potential toxicity, the circulation of iron is controlled in biological organs [3,4]. The shortage of iron leads to poor transportation of oxygen to living cells, resulting in weak immunity, whereas excessive concentration levels of iron in living cells catalyze the generation of active oxygen species [5-7]. These oxygen species cause changes in lipids, proteins, and nucleic acids. The toxic effects of iron on living cells usually cause acute disorders, such as Parkinson's, Alzheimer's, and Huntington's [8-10].

Many analytical methods have been described for the detection of poisonous iron(III), including voltammetry [11-13]. However, these traditional methods require trained personnel, tedious sample preparation, a sample destruction procedure, complicated instrumentation, time consumption, and/or high cost. Therefore, the simple colorimetric tools have been beneficial over other detection tools that require complicated instrumentation and/or procedures [14,15]. Colorimetric sensors have been widely used for the identification of harmful chemical agents, such as phenols, pesticides, and ammonia, due to their cost-effectiveness and ease of use, though sensitivity and selectivity depend on the probe used [16-18]. Therefore, scientists have recently focused on the development of efficient colorimetric detectors for iron(III) [19,20]. However, the preparation of a practical colorimetric detector for iron(III) has been a challenge due to the poor properties of synthetic probes, such as complicated preparation procedures, poor selectivity, weak sensitivity, and nonbiodegradability [21,22]. Solid-state sensors are characterized by operational simplicity, portability, and cheapness. Solid-state colorimetric sensors have been used as portable tools for laboratory and household assays [23]. In contrast to bulk materials, PCL/PLA nanofibrous membranes have shown a lightweight, high surface area, and better diffusion [24]. The non-cytotoxicity, high abundance, biodegradability, biocompatibility, renewability, and high absorption ability of PCL/PLA membranes make them promising for use in various fields, such as environmental and medicinal monitoring. Additionally, many reactive agents proved compatibility to produce simple composites of polycaprolactone/polylactic acid (PCL/PLA) [25]. Tannin is a biologically active polyphenol extracted from natural plants. It has various applications in tanning, metallurgy, foodstuffs, and cosmetics [26-29]. Tannin consists of plentiful phenolic hydroxyls, imparting remarkable biological and pharmacological activities, as well as excellent chemical and physical characteristics [30]. Tannin can interact with polysaccharides, metals, and proteins via coordination bonding to display different ecological and physiological impacts [31,32]. When the pH value is lower than its pKa value, tannin can also function as an active site for hydrogen bonding [33].

*Corresponding author:
*E-mail address:* sdalohtany@pnu.edu.sa (S. Al-Qahtani)

**Received:** 16 February, 2025 **Accepted:** 24 August, 2025 **Epub Ahead of Print:** 05 November 2025 **Published:** 14 November 2025
**DOI:** 10.25259/AJC_158_2025

Electrospinning is a cheap methodology for the formation of nanofibers from various materials, such as polymer composites [34-36]. Electrospun membranes are distinguished by a miniaturized diameter and high surface area. Additionally, a fiber diameter can be easily controlled by adjusting the spinning conditions and parameters [37]. Electrospun membranes have been employed in various fields, such as environmental remediation, tissue engineering, sensors and biosensors, filtration systems, solar cells, and protective clothing [38-43]. Herein, we present the development of electrospun tannin-encapsulated nanofibrous membranes from a tannin phenolic indicator as a spectroscopic probe and PCL/PLA as a hosting agent for the colorimetric identification of iron(III). The current tannin-encapsulated nanofibrous membrane with a high surface area can be used for efficient sensing purposes.

## 2. Materials and Methods

### 2.1. Materials

PLA (Mw 1.20 × $10^5$ g/mol, L-lactide content of 88%) and PCL (GPC: Mn ~10,000, Mw ~14,000) were provided by Sigma-Aldrich (Germany). The analytical grade chemicals were acquired from Merck (Germany), including sodium hydroxide, hydrochloric acid (37%), tannic acid (ACS reagent), and absolute ethanol. The heavy metal salts were purchased from Sigma-Aldrich (Germany), including $K_2SO_4$, NaCl, $CuCl_2$, $CoSO_4$, $BaCl_2$, $MgCl_2$, $HgCl_2$, $ZnCl_2$, $NiCl_2$, $CaCl_2$, $CdCl_2$, $MnCl_2$, $FeCl_3$, $CrCl_3$, and $AlCl_3$. The appropriate amounts of the metal salts were dissolved in distilled water to prepare stock aqueous solutions. The working solutions of the metal salts were prepared by diluting the respective stock solutions with distilled water.

### 2.2. Electrospinning of tannin@PCL/PLA

The PCL/PLA nanofibers were developed under ambient conditions according to previously presented procedures with slight modifications [25]. A mixture of PCL (70% w/w) and PLA (30% w/w) was dissolved in a mixture of dimethylformamide/chloroform (1:1 v/v) and stirred for 9 h. The provided solution was sonicated at 25 kHz for 20 min and then admixed with the tannin probe at various contents, including 0%, 0.5%, 1%, 1.5%, 2%, and 2.5% w/w of tannic acid to PCL/PLA. The produced solutions were represented by $TA_0$, $TA_1$, $TA_2$, $TA_3$, $TA_4$, and $TA_5$, respectively. The provided combinations were homogenized for 45 min. The electrospun nanofibers were injected from a plastic syringe (15 mL) filled with the spinnable fluid (10 mL). The produced nanofibers were dried in a vacuum oven at 45 °C. According to a previously reported method [39], the nanofibrous membranes were treated with oxygen plasma for 15 min to improve the membrane hydrophilicity and then placed in a dry box. Scanning electron microscopy (SEM) and energy-dispersive X-ray (EDX) were used to conduct the structural characterization of the produced fibers.

### 2.3. Electrospinning device

An electrospinning apparatus consists of a power source, a syringe pump, and a collector that is a 10 cm diameter and a 30 cm long grounded metal drum. A spinning speed of 180 rpm was used to collect the nanofibers under ambient conditions. The tannin-containing PCL/PLA solutions were released from a plastic syringe at a regulated flow rate of 0.9 mL/h, using a programmable pump. The plastic syringe had a needle tip (stainless steel; 1.27 mm) linked to a DC voltage supply. A high electric voltage of 30 kV was applied to ensure uniform nanofiber formation with controlled diameter and morphology. The collector was positioned at the exact middle of the syringe pump's needle tip. The collection system and the needle tip were spaced 20 cm apart to allow for better airflow. A wooden fume hood with a ventilation system was used to conduct the electrospinning operation at room temperature and humidity.

### 2.4. Colorimetric identification of iron(III)

The metallochromic membrane determined the presence of ferric under ambient conditions. The membrane had a thickness of 360 μm, a length of 2 cm, and a width of 2 cm. Various quantities of ferric chloride (0.5-125 ppm) were dissolved in distilled water at a pH of 7. The coloration measurements were determined after immersing the nanofibrous sensor film in aqueous solutions of $FeCl_3$ for 3-5 s. Moreover, aqueous media of other heavy metallic salts (125 ppm) were tested, including $K_2SO_4$, NaCl, $CaCl_2$, $CdCl_2$, $MnCl_2$, $BaCl_2$, $ZnCl_2$, $NiCl_2$, $HgCl_2$, $CoSO_4$, $CuCl_2$, $MgCl_2$, $CrCl_3$, and $AlCl_3$.

### 2.5. Characterization methods

#### 2.5.1. Morphological analysis

Using VEGA3 TESCAN (Czeck Republic), SEM images of the nanofibrous films were examined at an acceleration voltage of 20 kV and a resolution of 7-15 kx. ImageJ software was employed to measure the fibrous diameters on SEM images. Using EDX (TEAM Model) paired to SEM, we were able to assess the elemental compositions of the produced fibers. EDX analysis of $TA_4$ was performed before and after immersion in an aqueous solution of ferric ions. A JEM-2100 Plus (Tokyo, Japan) was employed to measure the structural features of the Tannin/$Fe^{3+}$ complex nanoparticles at an acceleration voltage of 200 kV.

#### 2.5.2. Mechanical screening

A FX-3300 Textest was employed to evaluate the air permeability, using standard procedures (ASTM D-737) [44]. The stiffness of tannin-encapsulated nanofibrous membranes was investigated by a Shirley stiffness apparatus, using a British procedure (3356:1961) [45].

#### 2.5.3. Colorimetric analysis

Using an Ultrascan Pro (HunterLab, U.S.A.), the coloration measurements of the fibrous membranes were studied. The color change was tracked by the color strength (*K/S*), CIE Lab space coordinates, and absorption spectra, where $b^*$ is the blue(–$b^*$)/yellow(+$b^*$) axis, $L^*$ is the white(100)/black(0) axis, and $a^*$ is the green(–$a^*$)/red(+$a^*$) axis [46].

#### 2.5.4. Statistical screening

The statistical analysis was reported by GraphPad Prism software (version 6.0, San Diego, CA, USA), using the one-way *ANOVA* calculation system. The experimental procedures were replicated thrice and the findings were recorded as the average ± standard deviation (SD).

## 3. Results and Discussion

### 3.1. Morphology of chromic fibers

Various contents of tannin were combined with a viscous solution of PCL/PLA. The viscous solutions were electrospun to create tannin-immobilized PCL/PLA membranes. The electrospun PCL/PLA formed a nanofibrous network with a high surface area. The morphology of the produced membrane was examined, as shown in Figure 1. SEM images showed that the tannin probe is embedded within the electrospun sensor nanofiber because no particles were detected on the fiber surface. The thin nanofibrous membrane showed a random orientation of its fibers and was highly sensitive to ferric ions. This high sensitivity is attributed to the good interconnectivity, high surface area, and high porosity of the assembled membrane. These characteristics allowed the analyte ($Fe^{3+}$) to diffuse throughout the mesh of a fibrous membrane to activate the tannin sites. The tannin-immobilized nanofibrous film was fabricated via electrospinning, optimizing tannin content, flow rate, collector distance, and applied voltage. The morphological and spinnability characteristics of the tannin-encapsulated PCL/PLA fibers were enhanced by changing these factors. A 3D porous film is the result of applying a high voltage to a viscous solution. A nonwoven mat was formed by the assembled fibers, which had diameters ranging from 100 to 350 nm for the tannin-free nanofibers ($TA_0$) and diameters ranging from 100 to 420 nm for the tannin-containing nanofibers ($TA_4$). When

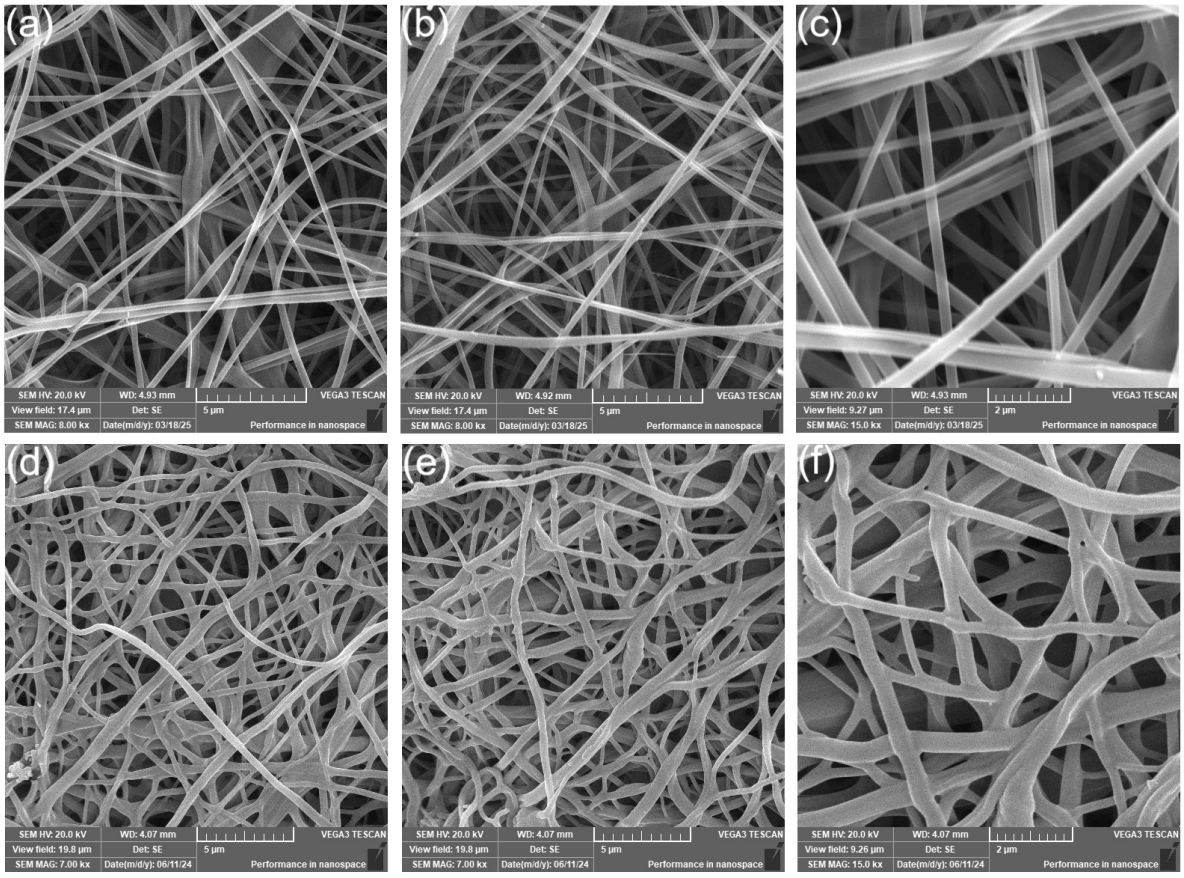


**Figure 1.** SEM images of electrospun nanofibrous membranes at different magnifications, including (a-c) $TA_0$ and (d-f) $TA_4$.

**Table 1.** EDX analysis of $TA_4$ before and after immersion in an aqueous medium of ferric chloride.

| Sample | Carbon | Oxygen | Iron |
|---|---|---|---|
| *Before* | 64.61 | 35.39 | – |
| *After* | 64.31 | 35.52 | 0.17 |

the tannin ratio was increased, no discernible alterations were observed in the morphology of the resulting nanofibers.

Table 1 shows the EDX analysis of the nanofibrous membrane ($TA_4$) before and after immersion in an aqueous medium of ferric chloride. Before exposure to ferric, both carbon and oxygen were detected by EDX due to the structure of PCL/PLA [24]. After exposure to ferric, carbon, iron, and oxygen were detected by EDX due to the structure of PCL/PLA and the presence of ferric analyte.

Both stiffness and breathability of the textile membranes were investigated. The membrane air permeability persisted unchanged with raising the tannin content (Figure 2a), whereas the stiffness slightly decreased with raising the tannin content (Figure 2b).

### 3.2. Analysis of metallochromism

Various concentrations of ferric chloride (0.5-125 ppm) in distilled water were prepared. The $TA_0$ sample remained colorless even when exposed to ferric ions. On the other hand, the transparent strips ($TA_x$; X = 1, 2, 3, 4, 5) became purple when exposed to varying amounts of ferric ions in aqueous media (Figures 3a,b). The $TA_x$ sensor was submerged in

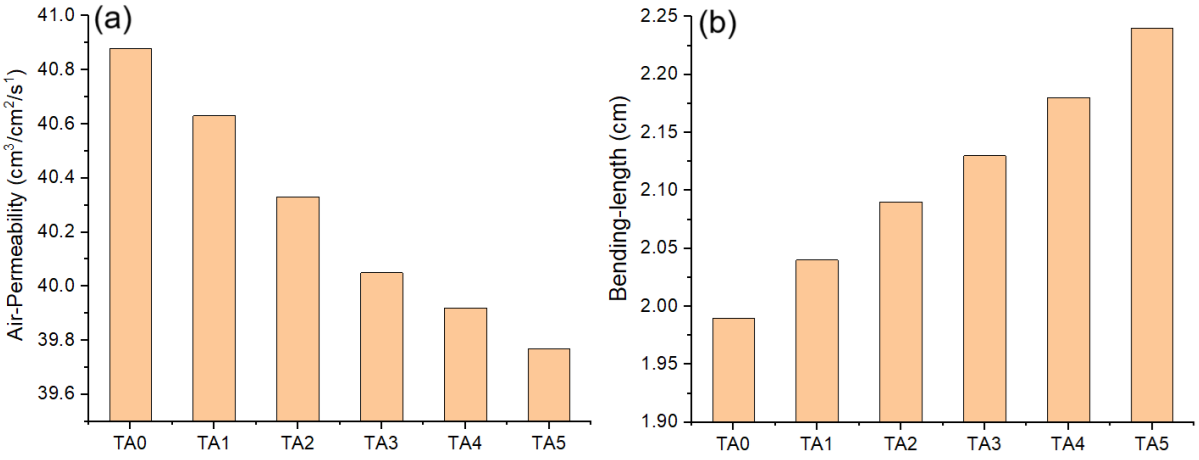


**Figure 2.** (a) Air permeability and (b) bending length for tannin-encapsulated nanofibers. The correlations are recognized high ($p \leq 0.001$).

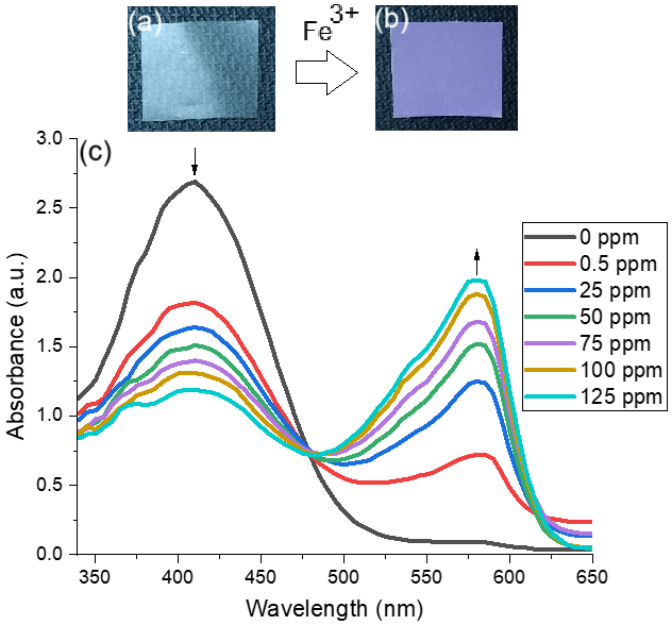


**Figure 3.** (a) Color change from transparent at ferric concentration of 0 ppm (b) to purple at ferric concentration of 125 ppm, and (c) UV-Vis absorption spectra for the $TA_4$ nanofibrous membrane after exposure to Fe(III) solutions at different concentrations (0.5-125 ppm), showing a bathochromic shift from 409 nm to 580 nm.

the aqueous ferric solution under ambient conditions for 3-5 seconds, causing a color change from colorless to purple as a function of increasing the iron(III) chloride concentration level from 0.5 to 125 ppm. As a function of the ferric concentration, different complexes with varying degrees of purple color are produced by forming a coordination bond between ferric ions and the phenolic tannin. To determine the harmful ferric concentrations between 0.5 and 125 ppm, a calibration profile curve was constructed by measuring their absorption intensities at 580 nm. Using the tannin-encapsulated PCL/PLA sensor, we were able to accurately measure an unknown concentration of ferric in an aqueous solution. Figure 3(c) illustrates the absorbance spectra of $TA_4$ as a function of the ferric concentration. The isosbestic point detected at 479 nm proved the presence of two different chemical structures, including Tannin/Fe(III) complex and tannic acid, with two different colors, including colorless and purple, respectively. The total amount of ferric chloride in water was determined by a correlation profile, as shown in Figure 3. An exponentially growing correlation profile was observed at 580 nm as the Fe(III) content increased from 0.5 to 125 ppm. The absorption intensity of $TA_4$ at 580 nm remained unchanged when the ferric concentration was reduced to below 0.5 ppm. This allowed for the monitoring of a detection limit as low as 0.5 ppm. Due to the development of a complex between Fe(III) and the tannin hydroxyl substituents, the color change was monitored as the quantity of Fe(III) increased. Based on the variations in absorbance intensity with increasing the Fe(III) content, the detection limit was determined to be as high as 125 ppm, beyond which no further increases in the absorbance intensity (at 580 nm) were observed. Thus, the absorbance intensity at 580 nm increased with Fe(III) concentration up to 125 ppm, beyond which saturation of binding sites was observed. Consequently, the current sensor is both simple and efficient, displaying a detection range of 0.5-125 ppm. A drinking tap water sample was tested by the $TA_4$ membrane to display an absorption wavelength of 580 nm with an intensity value of 0.769. Using the calibration curve shown in Figure 4, the iron content in the water sample was recorded at around 0.6 ppm. The results proved that the current metallochromic membrane can be used to efficiently determine the ferric content in real water samples. The absorption spectra have shown that the developed sensor provides the same optical results after storage for seven months, proving long-term stability.

An evaluation of the sensor efficiency must take both interference and selectivity into consideration. This study investigated the

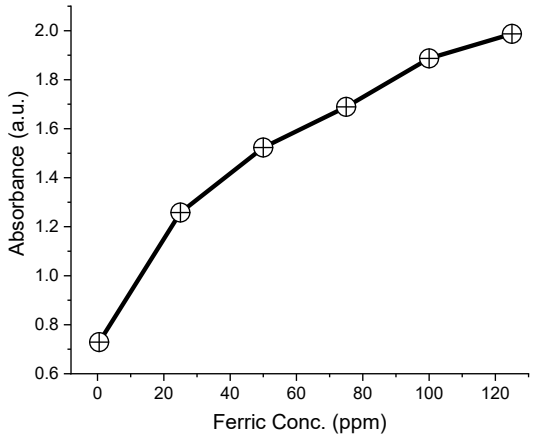


**Figure 4.** UV-Vis absorption spectra of the TA4 nanofibrous membrane after exposure to Fe(III) solutions at different concentrations (0.5-125 ppm), showing a bathochromic shift from 409 nm to 580 nm.

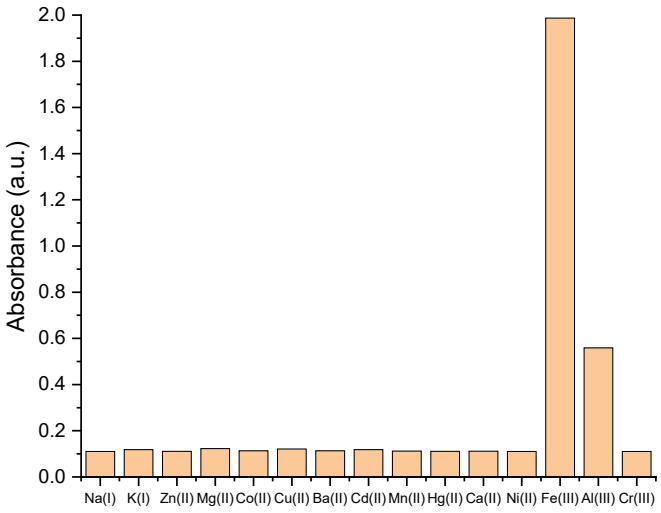


**Figure 5.** Absorption intensities of $TA_4$ at 580 nm for various competitive metal ions (125 ppm).

specificity of tannin-integrated PCL/PLA for Fe(III) by analyzing its behavior with various trivalent, divalent, and monovalent salts, such as $K^+$, $Na^+$, $Zn^{2+}$, $Cu^{2+}$, $Mn^{2+}$, $Hg^{2+}$, $Mg^{2+}$, $Cd^{2+}$, $Co^{2+}$, $Ca^{2+}$, $Ni^{2+}$, $Ba^{2+}$, $Al^{3+}$, and $Cr^{3+}$. Figures 3 and 4 show the absorbance spectra of $TA_4$ in the presence of $Fe^{3+}$, which exhibited an absorption wavelength of 580 nm. As illustrated in Figure 5, the absorption spectra of $TA_4$ displayed a maximum wavelength of 409 nm when no metal ions were present and when $K^+$, $Na^+$, $Co^{2+}$, $Mn^{2+}$, $Zn^{2+}$, $Ba^{2+}$, $Cd^{2+}$, $Ni^{2+}$, $Ca^{2+}$, $Cu^{2+}$, $Hg^{2+}$, $Mg^{2+}$, or $Cr^{3+}$ were present. As illustrated in the absorbance spectra at 580 nm, the tannin-encapsulated PCL/PLA sensor demonstrated an impressive increase in selectivity for ferric. The detector selectivity to $Fe^{3+}$ was confirmed when no significant changes were monitored in the absorbance spectra of other metal ions. However, $Al^{3+}$ demonstrated a modest degree of sensitivity to the tannin-encapsulated PCL/PLA sensor, having its absorbance spectra monitored at two distinct bands of 523 nm. This could be attributed to the variable capabilities of metal ions to establish coordinative bonds with the tannin hydroxyls [4]. Thus, evidently the tannin-encapsulated PCL/PLA sensor is useful for an easy and simple detection of Fe(III) in water by visual inspection. Figure 5 shows a comparison of the absorption intensity of $TA_4$ at 580 nm for some selected metal ions, with a constant concentration of 125 ppm. The sensor tool can be used for both quantitative and qualitative identification of the harmful $Fe^{3+}$, since the competing ions showed negligible effects on $TA_4$. The present film eliminates the need for complicated instrumental analysis by providing a straightforward method for naked-eye and real-time determination of $Fe^{3+}$.

**Table 2.** Coloration screening of sensory membranes.

| Membrane | L* | a* | b* | *K/S* |
|---|---|---|---|---|
| $TA_0$ | 92.35 | 2.74 | 1.62 | 0.65 |
| $TA_1$ | 86.02 | 2.10 | 2.36 | 0.94 |
| $TA_2$ | 82.19 | 1.98 | 3.27 | 1.19 |
| $TA_3$ | 79.83 | 1.61 | 4.14 | 1.43 |
| $TA_4$ | 78.95 | 1.47 | 4.55 | 1.77 |
| $TA_5$ | 78.74 | 1.22 | 4.76 | 1.82 |

Evaluation of the sensing efficiency was determined by measuring both CIE Lab and *K/S* (Table 2). When the overall amount of the tannin biomolecule was increased, a negligible increase in *K/S* was monitored. Based on the tannin concentration, the nanofibrous membranes showed a wide range of colorimetric parameter values. Increasing the tannin concentration causes a significant reduction in the L* value, verifying a slightly darker color. The positive value of a* dropped while the positive value of b* rose when the concentration of tannin increased. There were no discernible alterations in CIE Lab and *K/S* when the tannin content was raised from $TA_4$ to $TA_5$. Thus, the sensor performance of $TA_4$ showed the optimum colorimetric properties among the tannin-encapsulated PCL/PLA samples. As shown in Table 3, the $TA_4$ sensor was tested for the determination of $Fe^{3+}$ relative to many other metal ions (125 ppm). When immersed in separate solutions of $Na^+$, $K^+$, $Cu^{2+}$, $Zn^{2+}$, $Co^{2+}$, $Mn^{2+}$, $Ni^{2+}$, $Cd^{2+}$, $Hg^{2+}$, $Ba^{2+}$, $Ca^{2+}$, $Mg^{2+}$, or $Cr^{3+}$, the $TA_4$ sensor showed relatively minor variations in CIE Lab and *K/S*. However, $Al^{3+}$ exhibited weak sensitivity to the tannin-immobilized PCL/PLA sensor as compared to $Fe^{3+}$. The color strength of $TA_4$ was improved in the presence of ferric.

### 3.3. Effect of pH

Changing the pH has a noticeable effect on tannin and $Fe^{3+}$ ions. A stock solution (125 ppm) of $Fe^{3+}$ in water was prepared. By adding appropriate amounts from aqueous solutions of NaOH (1 M) and HCl (1 M), the pH was adjusted within a range of 4.0-6.5. The produced solutions with varying pH levels had their absorbance spectra measured. For every solution, the absorbance intensity was recorded. Figure 6 shows a graph of the absorbance intensity with increasing pH value. Because $Fe^{3+}$ has a high rate of coagulation in the extremely low pH range (highly acidic medium) [47], there were no discernible variations in the absorbance intensity of Tannin/$Fe^{3+}$ at pH values below 4.0 and above 6.5. Above a pH value of 6.5, the tannin molecules form electrolyte complexes with cations by acting as a stiff anion [48].

**Table 3.** Colorimetric coordinates of $TA_4$ in the presence of different metal salts (125 ppm).

| Salt | L* | a* | b* | *K/S* |
|---|---|---|---|---|
| **Fe(III)** | 46.92 | 12.7 | –9.39 | 6.76 |
| **Al(III)** | 59.87 | 7.21 | –5.77 | 2.02 |
| **Cr(III)** | 78.62 | 1.43 | 4.46 | 1.63 |
| **Cd(II)** | 76.63 | 1.37 | 4.52 | 1.88 |
| **Cu(II)** | 71.39 | 1.45 | 4.63 | 1.67 |
| **Mn(II)** | 79.73 | 1.54 | 4.59 | 1.73 |
| **Mg(II)** | 77.35 | 1.48 | 4.13 | 1.69 |
| **Ba(II)** | 79.2 | 1.45 | 4.38 | 1.71 |
| **Zn(II)** | 78.75 | 1.49 | 4.88 | 1.63 |
| **Co(II)** | 77.92 | 1.63 | 4.23 | 1.64 |
| **Ca(II)** | 79.16 | 1.48 | 4.24 | 1.56 |
| **Hg(II)** | 77.77 | 1.53 | 4.3 | 1.59 |
| **Ni (II)** | 76.56 | 1.42 | 4.31 | 1.82 |
| **Na(I)** | 79.59 | 1.41 | 4.77 | 1.86 |
| **K(I)** | 79.07 | 1.57 | 4.55 | 1.71 |

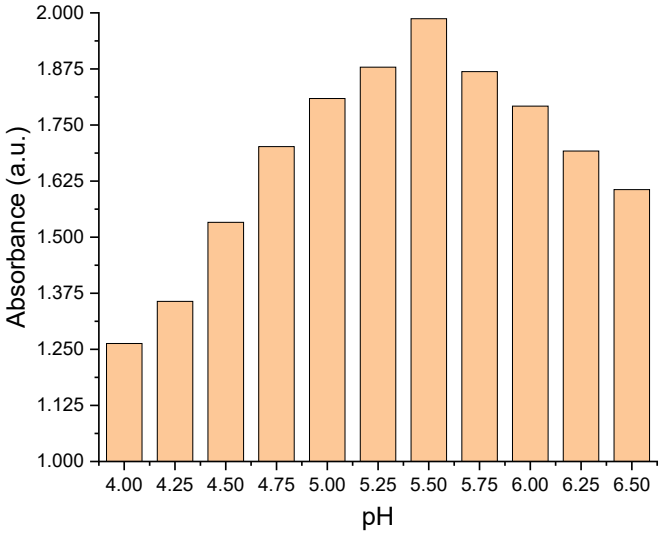


**Figure 6.** Impact of pH on the absorption intensity of $TA_4$ at 580 nm upon detecting $Fe^{3+}$ (conc. 125 ppm).

With a very acidic pH<4.0, this coagulation prevents the adsorption and diffusion of ferric throughout the tannin-encapsulated PCL/PLA film. Contrarily, an increase in absorption intensity was monitored in the pH range of 4.0-6.5, suggesting a wide variety of possible binding sites for $Fe^{3+}$ with the tannin sites. The tannin molecular structure has several hydroxyl substituents that can function as coordinating sites. Therefore, tannin-encapsulated PCL/PLA can be used as a selective detector for $Fe^{3+}$ in the pH range of 4.0-6.5.

### 3.4. Mechanism of metallochromism

Quantitative and qualitative identification of ferric ions in water was achieved by forming a Tannin/$Fe^{3+}$ coordination complex, which changes the tannin color. The current phenolic tannin-encapsulated PCL/PLA test strip can detect ferric ions in a real water sample. It was primarily the ferric content that caused the color (bathochromic) shift from colorless to pale and dark purple. Tannin is supposed to interact with the backbone of PCL/PLA via hydrogen bonding [49]. Tannin consists of a central glucose unit derivatized with ten galloyl moieties that can act as chromophore sites. Biophenols have proven to be effective binding agents for ferric [27-29]. The coordination binding between tannin and ferric generates a highly stable complex that acquires a purple color. Thus, the current nanofibrous membranes can function as a metallochromic selective probe by switching color upon coordination binding with $Fe^{3+}$ in aqueous media. The tannin indicator inside the nanofibrous film underwent a partial chromogenic reaction at low total Fe(III) concentrations owing to partial coordination of tannin hydroxyls with $Fe^{3+}$. It was observed that the degree of coordination improved as the Fe(III) concentration rose. The degree to which the tannin indicator and Fe(III) are coordinated determines the spectrum of colors produced by the $TA_4$ sensor, as depicted in Figure 7. The metal-polyphenol coordination bonding depends on the covalent character of the coordinate bond, the intrinsic basicity of donor atoms (polyphenol), and the coulombic repulsion and attraction of charged groups and ions. In coordination bonds, the polyphenol (tannin) electrons are donated to the metal (ferric) to generate a molecular orbital with a dipole moment, which distorts the d orbitals of the metal ion. Additionally, the formation of a coordinate bond depends on the relative entropy and enthalpy changes upon binding a multidentate ligand [4,45]. The isosbestic point determined at 479 nm verified the presence of two different chemical structures, including Tannin/$Fe^{3+}$ coordination complex and tannic acid, with two different colors, including colorless and purple, respectively.

The establishment of Tannin/$Fe^{3+}$ coordinative nanoparticles was verified by the dropwise addition of $FeCl_{3(aq)}$ (0.1 M) to an aqueous solution of tannin (0.1 M). The Tannin/$Fe^{3+}$ coordinative nanoparticles were formed after an hour of vigorous stirring under ambient conditions.

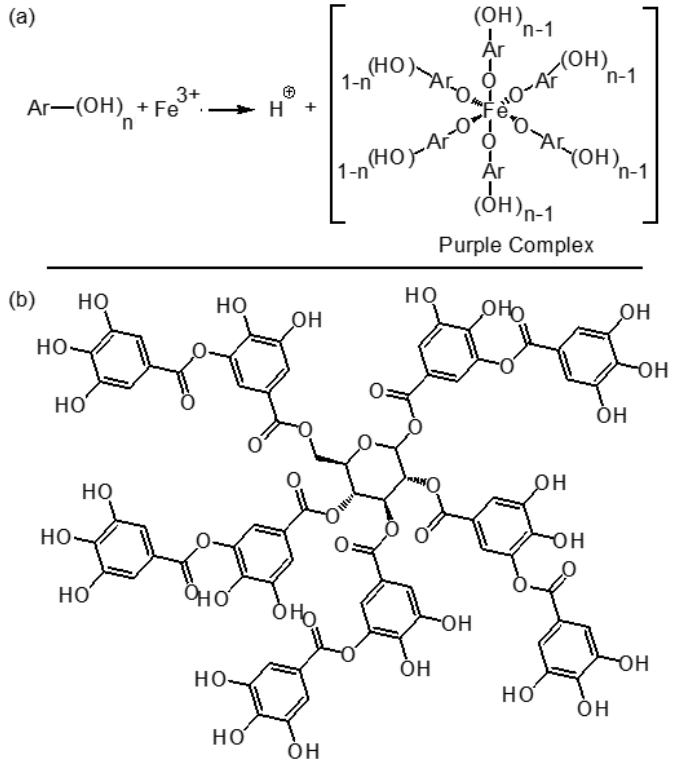


**Figure 7.** (a) Proposed mechanism for the metallochromic interaction to generate a colored complex, and (b) molecular structure of tannin.

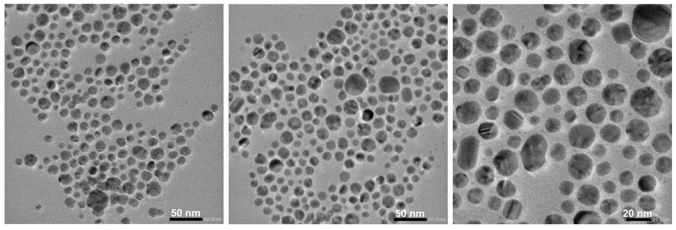


**Figure 8.** TEM analysis of Tannin/$Fe^{3+}$ coordinative nanoparticles at different locations on the sample.

Figure 8 displays the transmission electron microscope (TEM) analysis of Tannin/$Fe^{3+}$ coordinative nanoparticles, indicating diameters of 6-23 nm.

Heavy metals, such as iron, have been major contaminants in water sources. Thus, many analytical methods have been described for the adsorption and detection of poisonous heavy metals [50-54]. Iron has been the most prevalent heavy metal in the human body [1-7]. Graphene quantum dots functionalized with dopamine [55], silver nanoparticles functionalized with pyrophosphate [56], interferometric optical fiber functionalized with carbon dots [57], lanthanide metal-organic framework [58], nanoparticles of both gold and silver [59,60], tannin-integrated 3-aminopropyltriethoxysilane [61], and 2-(2′-pyridyl) imidazole-immobilized nanofibers framework [62] are among the sensors that have been presented for the identification of $Fe^{3+}$ in water. However, these material indicators are non-biodegradable, hazardous to both human health and environment, expensive, non-selective, slow, and difficult to prepare. In the current study, both PCL/PLA and tannin are nontoxic, environmentally friendly and biodegradable materials [27,28,63,64]. It has only come to light that colorimetric sensors provide a simple, effective, and inexpensive technology to detect various analytes [65-68]. Therefore, the natural tannin has the potential to be a very sensitive and selective colorimetric indicator for ferric ions. It is biodegradable and requires just a few basic steps to be extracted [32,33]. A limited number of studies have detailed the use of tannin as a ferric ion sensor with low sensitivity [11-15]. Herein, a detection range of 0.5-125 ppm was achieved by the present membrane, which can be employed as a portable detector. The maximum contamination level of iron in drinking water is 0.30 ppm [69]. Thus, the current tannin-encapsulated PCL/PLA membrane with a detection limit of 0.5 ppm can be considered as a practical sensory tool for the identification of iron toxicity in drinking water.

## 4. Conclusions

A novel colorimetric tannin-activated nanofibrous PCL/PLA metallochromic sensor was developed for the detection of Fe(III) ions. The current nanofibrous detector is characterized by sensitivity, selectivity, simplicity, quick detection, low cost, and portability. A spectroscopic probe encapsulated in a PCL/PLA nanofibrous (100-420 nm) host was the main key to the detection procedure. Depending on the quantity of Fe(III), the colorless (409 nm) sensor device changes color (bathochromic shift) to pale or dark purple (580 nm) in an aqueous environment within the pH range of 4.0-6.5. The current detection methodology proved to be a rapid method for real-time identification of $Fe^{3+}$. In comparison to other metal ions, including $Na^{+}$, $K^{+}$, $Zn^{2+}$, $Ca^{2+}$, $Cd^{2+}$, $Cu^{2+}$, $Ni^{2+}$, $Mn^{2+}$, $Ba^{2+}$, $Hg^{2+}$, $Mg^{2+}$, $Co^{2+}$, $Al^{3+}$, and $Cr^{3+}$, the nanofibrous tannin-encapsulated PCL/PLA sensor demonstrated a high degree of selectivity for the identification of $Fe^{3+}$. A detection range was tracked from 0.5 to 125 ppm. The generation of a Tannin/$Fe^{3+}$ complex was the main factor in the identification technique. TEM analysis of Tannin/$Fe^{3+}$ coordinative nanoparticles displayed diameters of 6-23 nm. The present detector has proven a real-time colorimetric determination of iron(III) without the necessity for complications and skilled personnel and/or procedures, in contrast to other detection technologies that have been previously reported. These necessitate electronic components and/or advanced equipment and/or procedures. However, future research should focus on enhancing the detection limit below 0.5 ppm using more sensitive nanostructures or functionalized probes. Additionally, the sensor functions within a pH range of 4.0-6.5. Thus, it should be improved to function in a wider pH range.

## CRediT authorship contribution statement

**Ghadah M. Al-Senani:** Conceptualization, Supervision, Validation, Data curation, Software, Methodology, Visualization, Investigation, Writing, Original draft preparation, Writing-Reviewing and Editing. **Salhah D. Al-Qahtani:** Methodology, Data curation, Software, Validation, Writing-Reviewing and Editing. **Hesah M. AlMohisen:** Conceptualization, Methodology, Visualization, Investigation, Data curation, Validation, Writing-Reviewing and Editing.

## Declaration of competing interest

The authors declare that they have no competing interests.

## Data availability

The data that support the findings of this study are available from the corresponding author upon reasonable request.

## Declaration of Generative AI and AI-assisted technologies in the writing process

The authors confirm that there was no use of artificial intelligence (AI)-assisted technology for assisting in the writing or editing of the manuscript and no images were manipulated using AI.

## Acknowledgment

Princess Nourah bint Abdulrahman University Researchers Supporting Project number (PNURSP2025R122), Princess Nourah bint Abdulrahman University, Riyadh, Saudi Arabia.

## References


1. Cadmus, P., Brinkman, S.F., May, M.K., 2018. Chronic toxicity of ferric iron for North American aquatic organisms: Derivation of a chronic water quality criterion using single species and mesocosm data. *Archives of Environmental Contamination and Toxicology*, **74**, 605-615. https://doi.org/10.1007/s00244-018-0505-2
2. Zaid, A., Ahmad, B., Jaleel, H., Wani, S.H., Hasanuzzaman, M. A critical review on iron toxicity and tolerance in plants: Role of exogenous phytoprotectants. In: *Plant Micronutrients*(Cham: Springer International Publishing), 83-99. https://doi.org/10.1007/978-3-030-49856-6_4
3. Wang, R., Xu, S.Y., Zhang, M., Ghulam, A., Dai, C.L., Zheng, P., 2020. Iron as electron donor for denitrification: The efficiency, toxicity and mechanism. *Ecotoxicology and Environmental Safety*, **194**, 110343. https://doi.org/10.1016/j.ecoenv.2020.110343
4. El-Naggar, M.E., El-Newehy, M.H., Aldalbahi, A., Salem, W.M., Khattab, T.A., 2021. Immobilization of anthocyanin extract from red-cabbage into electrospun polyvinyl alcohol nanofibers for colorimetric selective detection of ferric ions. *Journal of Environmental Chemical Engineering*, **9**, 105072. https://doi.org/10.1016/j.jece.2021.105072
5. Kirk, G.J.D., Manwaring, H.R., Ueda, Y., Semwal, V.K., Wissuwa, M., 2022. Below-ground plant–soil interactions affecting adaptations of rice to iron toxicity. *Plant, Cell & Environment*, **45**, 705-718. https://doi.org/10.1111/pce.14199
6. Zahra, N., Hafeez, M.B., Shaukat, K., Wahid, A., Hasanuzzaman, M., 2021. Fe toxicity in plants: Impacts and remediation. *Physiologia Plantarum*, **173**, 201-222. https://doi.org/10.1111/ppl.13361
7. Sotero-Santos, R.B., Rocha, O., Povinelli, J., 2007. Toxicity of ferric chloride sludge to aquatic organisms. *Chemosphere*, **68**, 628-636. https://doi.org/10.1016/j.chemosphere.2007.02.049
8. Pereira, A.C., Gonçalves, B.B., Brito, R.D.S., Vieira, L.G., Lima, E.C.O., Rocha, T.L., 2020. Comparative developmental toxicity of iron oxide nanoparticles and ferric chloride to zebrafish (Danio rerio) after static and semi-static exposure. *Chemosphere*, **254**, 126792. https://doi.org/10.1016/j.chemosphere.2020.126792
9. De Dorlodot, S., Lutts, S., Bertin, P., 2005. Effects of ferrous iron toxicity on the growth and mineral composition of an interspecific rice. *Journal of Plant Nutrition*, **28**, 1-20. https://doi.org/10.1081/pln-200042144
10. Altamura, S., Muckenthaler, M.U., 2009. Iron toxicity in diseases of aging: Alzheimer's disease, parkinson's disease and atherosclerosis. *Journal of Alzheimer's Disease*, **16**, 879-895. https://doi.org/10.3233/jad-2009-1010
11. Paut, A., Prkić, A., Mitar, I., Bošković, P., Jozić, D., Jakić, M., Vukušić, T., 2021. Potentiometric response of solid-state sensors based on ferric phosphate for iron(III) determination. *Sensors (Basel, Switzerland)*, **21**, 1612. https://doi.org/10.3390/s21051612
12. Chakraborty, S., Mandal, M., Rayalu, S., 2020. Detection of iron (III) by chemo and fluoro-sensing technology. *Inorganic Chemistry Communications*, **121**, 108189. https://doi.org/10.1016/j.inoche.2020.108189
13. Li, Z., Hou, J.T., Wang, S., Zhu, L., He, X., Shen, J., 2022. Recent advances of luminescent sensors for iron and copper: Platforms, mechanisms, and bio-applications. *Coordination Chemistry Reviews*, **469**, 214695. https://doi.org/10.1016/j.ccr.2022.214695
14. Cai, Y., Zhang, J., Zhang, M., Wang, M., Zhao, Y., 2022. The optical fiber sensing platform for ferric ions detection: A practical application for carbon quantum dots. *Sensors and Actuators B: Chemical*, **364**, 131857. https://doi.org/10.1016/j.snb.2022.131857
15. Alberti, G., Zanoni, C., Magnaghi, L.R., Biesuz, R., 2022. Deferoxamine-based materials and sensors for Fe(III) detection. *Chemosensors*, **10**, 468. https://doi.org/10.3390/chemosensors10110468
16. Liu, B., Zhuang, J., Wei, G., 2020. Recent advances in the design of colorimetric sensors for environmental monitoring. *Environmental Science: Nano*, **7**, 2195-2213. https://doi.org/10.1039/d0en00449a
17. Sun, J., Lu, Y., He, L., Pang, J., Yang, F., Liu, Y., 2020. Colorimetric sensor array based on gold nanoparticles: Design principles and recent advances. *TrAC Trends in Analytical Chemistry*, **122**, 115754. https://doi.org/10.1016/j.trac.2019.115754
18. Ye, M.L., Zhu, Y., Lu, Y., Gan, L., Zhang, Y., Zhao, Y.G., 2021. Magnetic nanomaterials with unique nanozymes-like characteristics for colorimetric sensors: A review. *Talanta*, **230**, 122299. https://doi.org/10.1016/j.talanta.2021.122299
19. Ali, Z., Ullah, R., Tuzen, M., Ullah, S., Rahim, A., Saleh, T.A., 2023. Colorimetric sensing of heavy metals on metal doped metal oxide nanocomposites: A review. *Trends in Environmental Analytical Chemistry*, **37**, e00187. https://doi.org/10.1016/j.teac.2022.e00187
20. Yu, L., Song, Z., Peng, J., Yang, M., Zhi, H., He, H., 2020. Progress of gold nanomaterials for colorimetric sensing based on different strategies. *TrAC Trends in Analytical Chemistry*, **127**, 115880. https://doi.org/10.1016/j.trac.2020.115880
21. Chen, W., Liang, H., Wen, X., Li, Z., Xiong, H., Tian, Q., Yan, M., Tan, Y., Royal, G., 2022. Synchronous colorimetric determination of $CN^-$, $F^-$, and $H_2PO_4^-$ based on structural manipulation of hydrazone sensors. *Inorganica Chimica Acta*, **532**, 120760. https://doi.org/10.1016/j.ica.2021.120760
22. Nguyen, V.N., Ha, J., Cho, M., Li, H., Swamy, K.M.K., Yoon, J., 2021. Recent developments of BODIPY-based colorimetric and fluorescent probes for the detection of reactive oxygen/nitrogen species and cancer diagnosis. *Coordination Chemistry Reviews*, **439**, 213936. https://doi.org/10.1016/j.ccr.2021.213936
23. Singh, R., Thakur, P., Thakur, A., Kumar, H., Chawla, P., V. Rohit, J., Kaushik, R., Kumar, N., 2021. Colorimetric sensing approaches of surface-modified gold and silver nanoparticles for detection of residual pesticides: A review. *International Journal of Environmental Analytical Chemistry*, **101**, 3006-3022. https://doi.org/10.1080/03067319.2020.1715382
24. Shi, C., Zhou, A., Fang, D., Lu, T., Wang, J., Song, Y., Lyu, L., Wu, W., Huang, C., Li, W., 2022. Oregano essential oil/β-cyclodextrin inclusion compound polylactic acid/polycaprolactone electrospun nanofibers for active food packaging. *Chemical Engineering Journal*, **445**, 136746. https://doi.org/10.1016/j.cej.2022.136746
25. Tambrchi, P., Mahdavi, A.H., DaliriJoupari, M., Soltani, L., 2022. Polycaprolactone-co-polylactic acid nanofiber scaffold in combination with 5-azacytidine and transforming growth factor-β to induce cardiomyocyte differentiation of adipose-derived mesenchymal stem cells. *Cell Biochemistry and Function*, **40**, 668-682. https://doi.org/10.1002/cbf.3728
26. Yan, W., Shi, M., Dong, C., Liu, L., Gao, C., 2020. Applications of tannic acid in membrane technologies: A review. *Advances in Colloid and Interface Science*, **284**, 102267. https://doi.org/10.1016/j.cis.2020.102267
27. Guo, Z., Xie, W., Lu, J., Guo, X., Xu, J., Xu, W., Chi, Y., Takuya, N., Wu, H., Zhao, L., 2021. Tannic acid-based metal phenolic networks for bio-applications: A review. *Journal of Materials Chemistry. B*, **9**, 4098-4110. https://doi.org/10.1039/d1tb00383f
28. Chen, C., Yang, H., Yang, X., Ma, Q., 2022. Tannic acid: A crosslinker leading to versatile functional polymeric networks: A review. *RSC Advances*, **12**, 7689-7711. https://doi.org/10.1039/d1ra07657d
29. Baer-Dubowska, W., Szaefer, H., Majchrzak-Celińska, A., Krajka-Kuźniak, V., 2020. Tannic acid: Specific form of tannins in cancer chemoprevention and therapy-old and new applications. *Current Pharmacology Reports*, **6**, 28-37. https://doi.org/10.1007/s40495-020-00211-y
30. Zhang, W., Roy, S., Ezati, P., Yang, D.-P., Rhim, J.-W., 2023. Tannic acid: A green crosslinker for biopolymer-based food packaging films. *Trends in Food Science & Technology*, **136**, 11-23. https://doi.org/10.1016/j.tifs.2023.04.004
31. Zaidi, S.F.A., Kim, Y.A., Saeed, A., Sarwar, N., Lee, N.E., Yoon, D.H., Lim, B., Lee, J.H., 2022. Tannic acid modified antifreezing gelatin organohydrogel for low modulus, high toughness, and sensitive flexible strain sensor. *International Journal of Biological Macromolecules*, **209**, 1665-1675. https://doi.org/10.1016/j.ijbiomac.2022.04.099
32. Zhang, W., Yang, Z.Y., Tang, R.C., Guan, J.P., Qiao, Y.F., 2020. Application of tannic acid and ferrous ion complex as eco-friendly flame retardant and antibacterial agents for silk. *Journal of Cleaner Production*, **250**, 119545. https://doi.org/10.1016/j.jclepro.2019.119545
33. Kaczmarek, B., Wekwejt, M., Nadolna, K., Owczarek, A., Mazur, O., Pałubicka, A., 2020. The mechanical properties and bactericidal degradation effectiveness of tannic acid-based thin films for wound care. *Journal of the Mechanical Behavior of Biomedical Materials*, **110**, 103916. https://doi.org/10.1016/j.jmbbm.2020.103916
34. Nadaf, A., Gupta, A., Hasan, N., Fauziya, N., Ahmad, S., Kesharwani, P., Ahmad, F.J., 2022. Recent update on electrospinning and electrospun nanofibers: Current trends and their applications. *RSC Advances*, **12**, 23808-23828. https://doi.org/10.1039/d2ra02864f
35. Bavatharani, C., Muthusankar, E., Wabaidur, S.M., Alothman, Z.A., Alsheetan, K.M., AL-Anazy, M., Ragupathy, D., 2021. Electrospinning technique for production of polyaniline nanocomposites/nanofibres for multi-functional applications: A review. *Synthetic Metals*, **271**, 116609. https://doi.org/10.1016/j.synthmet.2020.116609
36. Li, Y., Zhu, J., Cheng, H., Li, G., Cho, H., Jiang, M., Gao, Q., Zhang, X., 2021. Developments of advanced electrospinning techniques: A critical review. *Advanced Materials Technologies*, **6**, 1-29. https://doi.org/10.1002/admt.202100410
37. Luraghi, A., Peri, F., Moroni, L., 2021. Electrospinning for drug delivery applications: A review. *Journal of Controlled Release: Official Journal of the Controlled Release Society*, **334**, 463-484. https://doi.org/10.1016/j.jconrel.2021.03.033
38. Vass, P., Szabó, E., Domokos, A., Hirsch, E., Galata, D., Farkas, B., Démuth, B., Andersen, S.K., Vigh, T., Verreck, G., Marosi, G., 2020. Scale-up of electrospinning technology: Applications in the pharmaceutical industry. Wiley Interdisciplinary Reviews: *Nanomedicine and Nanobiotechnology*, **12**, e1611. https://doi.org/10.1002/wnan.1611
39. Al-Qahtani, S.D., Al-Senani, G.M., 2024. Development of toxic gas sensor from anthocyanin-embedded polycaprolactone-co-polylactic acid nanofibrous mat. *International Journal of Biological Macromolecules*, **267**, 131649. https://doi.org/10.1016/j.ijbiomac.2024.131649
40. Yang, X., Wang, J., Guo, H., Liu, L., Xu, W., Duan, G., 2020. Structural design toward functional materials by electrospinning: A review. *e-Polymers*, **20**, 682-712. https://doi.org/10.1515/epoly-2020-0068
41. Guo, Y., Wang, X., Shen, Y., Dong, K., Shen, L., Alzalab, A.A.A., 2022. Research progress, models and simulation of electrospinning technology: A review. *Journal of Materials Science*, **57**, 58-104. https://doi.org/10.1007/s10853-021-06575-w
42. Rahmati, M., Mills, D.K., Urbanska, A.M., Saeb, M.R., Venugopal, J.R., Ramakrishna, S., Mozafari, M., 2021. Electrospinning for tissue engineering applications. *Progress in Materials Science*, **117**, 100721. https://doi.org/10.1016/j.pmatsci.2020.100721
43. Al-Senani, G.M., Al-Qahtani, S.D., 2024. Preparation of transparent electrospun nanofibrous membrane from long-persistent phosphor-reinforced polymer for security authentication. *Journal of Applied Polymer Science*, **141**, e55472. http://doi.org/10.1002/app.55472
44. Hong, H.R., Kim, J., 2023. Nanoroughness-mediated bacterial adhesion on fabrics. *ACS Applied Nano Materials*, **6**, 18518-18530. https://doi.org/10.1021/acsanm.3c04015
45. Hassan, N.F., Khattab, T.A., Fouda, M.M.G., Abu Zaid, A.S., Aboshanab, K.M., 2024. Electrospun cellulose nanofibers immobilized with anthocyanin extract for colorimetric determination of bacteria. *International Journal of Biological Macromolecules*, **257**, 128817. https://doi.org/10.1016/j.ijbiomac.2023.128817
46. Binyaseen, A.M., Alaysuy, O., Alhasani, M., Sallam, S., Alkhatib, F., Alkhamis, K., Shah, R., El-Metwaly, N.M., 2024. Novel strategy toward color-tunable and glow-in-the-dark colorless smart natural wooden window. *Journal of Photochemistry and Photobiology A: Chemistry*, **448**, 115321. https://doi.org/10.1016/j.jphotochem.2023.115321
47. Lin, D., Bai, L., Gan, Z., Zhao, J., Li, G., Aminabhavi, T.M., Liang, H., 2020. The role of ferric coagulant on gypsum scaling and ion interception efficiency in

nanofiltration at different pH values: Performance and mechanism. *Water Research*, **175**, 115695. https://doi.org/10.1016/j.watres.2020.115695
48. Li, Y., Lin, R., Lv, F., Zhao, X., Yong, T., Zuo, X., 2022. Tannic acid-Fe complex derivative-modified electrode with pH regulating function for environmental remediation by electro-Fenton process. *Environmental Research*, **204**, 111994. https://doi.org/10.1016/j.envres.2021.111994
49. Gao, Y., Peng, X., Wu, Q., Yang, D., Wang, W., Peng, Q., Wang, T., Wang, J., Liu, J., Zhang, H., Zeng, H., 2022. Hydrogen-bonding-driven multifunctional polymer hydrogel networks based on tannic acid. *ACS Applied Polymer Materials*, **4**, 1836-1845. https://doi.org/10.1021/acsapm.1c01724
50. Dong, X., Ye, B., Xiang, H., Yao, M., 2023. Kinetic and isotherm of competitive adsorption cadmium and lead onto *Saccharomyces cerevisiae* autoclaved cells. *Environmental Geochemistry and Health*, **45**, 4853-4865. https://doi.org/10.1007/s10653-023-01540-9
51. Pérez-Nava, A., Bedolla-Guzmán, S., García-Bassoco, D., Cuevas-Yáñez, E., Frontana-Uribe, B.A., Chacón-García, L., Valle-Sánchez, M., González-Campos, J.B., 2024. Dipyrromethanes grafting on a poly (vinyl alcohol) nanofibrous mat as naked-eye sensor/receptor for detection and removal of ionic pollutants from water. *Chemical Engineering and Processing - Process Intensification*, **197**, 109688. https://doi.org/10.1016/j.cep.2024.109688
52. Wang, Z., Luo, P., Zha, X., Xu, C., Kang, S., Zhou, M., Nover, D., Wang, Y., 2022. Overview assessment of risk evaluation and treatment technologies for heavy metal pollution of water and soil. *Journal of Cleaner Production*, **379**, 134043. https://doi.org/10.1016/j.jclepro.2022.134043
53. Adnan, M., Xiao, B., Ali, M.U., Xiao, P., Zhao, P., Wang, H., Bibi, S., 2024. Heavy metals pollution from smelting activities: A threat to soil and groundwater. *Ecotoxicology and Environmental Safety*, **274**, 116189. https://doi.org/10.1016/j.ecoenv.2024.116189
54. Alrefaee, S.H., Aljohani, M., Alkhamis, K., Shaaban, F., El-Desouky, M.G., El-Bindary, A.A., El-Bindary, M.A., 2023. Adsorption and effective removal of organophosphorus pesticides from aqueous solution via novel metal-organic framework: Adsorption isotherms, kinetics, and optimization via Box-Behnken design. *Journal of Molecular Liquids*, **384**, 122206. https://doi.org/10.1016/j.molliq.2023.122206
55. Dutta Chowdhury, A., Doong, R.A., 2016. Highly sensitive and selective detection of nanomolar ferric ions using dopamine functionalized graphene quantum dots. *ACS Applied Materials & Interfaces*, **8**, 21002-21010. https://doi.org/10.1021/acsami.6b06266
56. Chavada, V.D., Bhatt, N.M., Sanyal, M., Shrivastav, P.S., 2017. Pyrophosphate functionalized silver nanoparticles for colorimetric determination of deferiprone via competitive binding to Fe(III). *Microchimica Acta*, **184**, 4203-4208. https://doi.org/10.1007/s00604-017-2417-7
57. Yap, S.H.K., Chan, K.K., Zhang, G., Tjin, S.C., Yong, K.T., 2019. Carbon dot-functionalized interferometric optical fiber sensor for detection of ferric ions in biological samples. *ACS Applied Materials & Interfaces*, **11**, 28546-28553. https://doi.org/10.1021/acsami.9b08934
58. Rozenberga, L., Bloch, W., Gillam, T.A., Lancaster, D.G., Skinner, W., Krasowska, M., Blencowe, A., Beattie, D.A., 2024. Europium metal–organic framework polymer composites with enhanced luminescence and selective ferric ion sensing. *ACS Applied Polymer Materials*, **6**, 3544-3553. https://doi.org/10.1021/acsapm.4c00111
59. Borah, N., Kalita, A.J., Guha, A.K., Das, M.R., Tamuly, C., 2022. Highly selective, rapid and simple colorimetric detection of Fe3+in fortified foods by L-Cysteine modified AuNP. *Microchemical Journal*, **179**, 107480. https://doi.org/10.1016/j.microc.2022.107480
60. Dayanidhi, K., Eusuff, N.S., 2021. Distinctive detection of Fe 2+ and Fe 3+ by biosurfactant capped silver nanoparticles via naked eye colorimetric sensing. *New Journal of Chemistry*, **45**, 9936-9943. https://doi.org/10.1039/D1NJ01342D
61. Hussain, Z., Ullah, S., Yan, J., Wang, Z., Ullah, I., Ahmad, Z., Zhang, Y., Cao, Y., Wang, L., Mansoorianfar, M., Pei, R., 2022. Electrospun tannin-rich nanofibrous solid-state membrane for wastewater environmental monitoring and remediation. *Chemosphere*, **307**, 135810. https://doi.org/10.1016/j.chemosphere.2022.135810
62. Ondigo, D.A., Tshentu, Z.R., Torto, N., 2013. Electrospun nanofiber based colorimetric probe for rapid detection of $Fe^{2+}$ in water. *Analytica Chimica Acta*, **804**, 228-234. https://doi.org/10.1016/j.aca.2013.09.051
63. Rahmatabadi, D., Aberoumand, M., Soltanmohammadi, K., Soleyman, E., Ghasemi, I., Baniassadi, M., Abrinia, K., Bodaghi, M., Baghani, M., 2023. Toughening PVC with biocompatible PCL softeners for supreme mechanical properties, morphology, shape memory effects, and FFF printability. *Macromolecular Materials and Engineering*, **308**, 1-13. https://doi.org/10.1002/mame.202300114
64. Rahmatabadi, D., Soltanmohammadi, K., Aberoumand, M., Soleyman, E., Ghasemi, I., Baniassadi, M., Abrinia, K., Bodaghi, M., Baghani, M., 2024. 4D printing of porous PLA-TPU structures: Effect of applied deformation, loading mode and infill pattern on the shape memory performance. *Physica Scripta*, **99**, 025013. https://doi.org/10.1088/1402-4896/ad1957
65. Al-Qahtani, S.D., Attia, Y.A., Al-Senani, G.M., 2024. Development of biochromic paper strips from cellulose nanocrystals and anthocyanin extract from pomegranate (*Punica granatum L.*) for colorimetric determination of urea. *Journal of Applied Polymer Science*, **141**, e56284. https://doi.org/10.1002/app.56284
66. Khattab, T.A., 2018. Novel solvatochromic and halochromic sulfahydrazone molecular switch. *Journal of Molecular Structure*, **1169**, 96-102. https://doi.org/10.1016/j.molstruc.2018.05.048
67. Abdelrahman, M.S., Khattab, T.A., Kamel, S., 2021. Development of a novel colorimetric thermometer based on poly (N-vinylcaprolactam) with push–π–pull tricyanofuran hydrazone anion dye. *New Journal of Chemistry*, **45**, 5382-5390. https://doi.org/10.1039/D1NJ00221J
68. Al-Qahtani, S.D., Attia, Y.A., Al-Senani, G.M., 2024. Development of strontium aluminate-printed nonwoven fabric from recycled cotton cellulose for smart wearable photochromic applications. *Luminescence*, **39**, 1-11. https://doi.org/10.1002/bio.4903
69. Motshakeri, M., Angoro, B., Phillips, A.R.J., Svirskis, D., Kilmartin, P.A., Sharma, M., 2025. Advancements in mercury-free electrochemical sensors for iron detection: A decade of progress in electrode materials and modifications. *Sensors (Basel, Switzerland)*, **25**, 1474. https://doi.org/10.3390/s25051474